

Very high energy gamma radiation associated with the unshocked wind of the Crab pulsar

S.V. Bogovalov,¹ F.A. Aharonian^{2*}

¹ *Astrophysics Institute at the Moscow Engineering Physics Institute, Kashirskoe Shosse 31, Moscow 115409, Russia*

² *Max Planck Institut für Kernphysik, Postfach 103980, D-69029 Heidelberg, Germany*

Accepted 1999 November 10. Received 1999 November 10; in original form 1999 March 4

ABSTRACT

We show that the relativistic wind of the Crab pulsar, which is commonly thought to be invisible in the region upstream of the termination shock at $r \leq r_S \sim 0.1$ pc, in fact could be directly observed through its inverse Compton (IC) γ -ray emission. This radiation is caused by illumination of the wind by low-frequency photons emitted by the pulsar, and consists of two, *pulsed* and *unpulsed*, components associated with the nonthermal (pulsed) and thermal (unpulsed) low energy radiation of the pulsar, respectively. These two components of γ -radiation have distinct spectral characteristics, which depend essentially on the site of formation of the kinetic-energy-dominated wind, as well as on the Lorentz factor and the geometry of propagation of the wind. Thus, the search for such specific radiation components in the spectrum of the Crab Nebula can provide unique information about the unshocked pulsar wind that is not accessible at other wavelengths. In particular, we show that the comparison of the calculated flux of the unpulsed IC emission with the measured γ -ray flux of the Crab Nebula excludes the possibility of formation of a kinetic-energy-dominated wind within 5 light cylinder radii of the pulsar, $R_w \geq 5R_L$. The analysis of the pulsed IC emission, calculated under reasonable assumptions concerning the production site and angular distribution of the optical pulsed radiation, yields even tighter restrictions, namely $R_w \geq 30R_L$.

Key words: relativity - stars: individual: Crab pulsar - pulsars: general - ISM: individual: Crab Nebula - gamma-rays: observations Crab Nebula

1 INTRODUCTION

The Crab pulsar is a powerful nonthermal machine, accelerating plasma in the form of a relativistic wind that carries off most of the rotational energy of the pulsar.

At a distance of about $r = r_S \sim 0.1$ pc the wind is terminated by a standing reverse shock, which accelerates the electrons up to energies 10^{15} eV, and randomizes their pitch angles (Rees & Gunn 1974; Kennel & Coroniti 1984). This results in formation of a bright synchrotron source in the region downstream of the shock. The synchrotron radiation of the Crab Nebula is well studied in a very broad frequency range, from radio to hard X-rays. Its general spectral and spatial characteristics are satisfactorily explained by the relativistic magnetohydrodynamics (MHD) model of Kennel & Coroniti (1984). Remarkably, the latter provides also a reasonable explanation, even in its simplified (spherically symmetric) form, for the detected very high energy (VHE)

γ -rays as a result of inverse Compton (IC) scattering of relativistic electrons in the ambient low-frequency photon fields. This implies that the study of the TeV IC radiation of the Crab Nebula, combined with synchrotron X-ray emission, can yield unambiguous information about the relativistic electrons and the nebular magnetic field in the downstream region of the shock (de Jager & Harding 1992; Stepanian 1995; Atoyan & Aharonian, 1996; Hillas et al. 1998).

Although very important, this information unfortunately does not tell much about the origin and characteristics of the wind, i.e. about the region between the pulsar magnetosphere and the shock. It is generally believed that this region, where almost the whole rotational energy of the pulsar is somehow released in the form of kinetic energy of the wind, cannot be directly observed. This has a simple explanation. Although the wind electrons may have an energy as large as $\sim 10^{13}$ eV, they move together with the magnetic field and thus do not emit synchrotron radiation. This explains the fact that the region upstream of the shock is *underluminous* (Kennel & Coroniti 1984). However, this statement is valid only for the synchrotron radiation of the

* E-mail: Felix.Aharonian@mpi-hd.mpg.de

wind. In fact, the wind could be *directly* observed through its IC radiation. Indeed, the IC γ -radiation of the wind electrons is unavoidable because of the illumination of the wind by external low-energy photons of different origin. There are three isotropic photon field populations that contribute effectively to the production of IC γ -radiation of the nebula in the downstream region: the nonthermal (synchrotron) and thermal (dust) radiation of the Crab Nebula itself, and the 2.7 K microwave background radiation (Atoyan & Aharonian 1996). Formally, all these photon fields could also serve as a target for the IC scattering of the wind before the shock. However, the fluxes of γ -rays emitted through these channels appear to be well below the sensitivity threshold of γ -ray telescopes. Meanwhile, in the pulsar vicinity, namely within approximately 100 light cylinders, the efficiency of production of IC γ -rays dramatically increases because of the existence of intense low energy radiation of the pulsar itself. The radiation consists of two, pulsed and unpulsed components, the latter being modulated at the period of the pulsar.

In this paper we show that at certain circumstances concerning the position of formation of the particle dominated wind, the geometry of the flow and the Lorentz-factor of the bulk motion of the wind, the fluxes of the IC γ -radiation of the wind could be sufficiently high to enable detection by present and forthcoming space-borne and ground-based γ -ray telescopes. Moreover, the distinct spectral features of this radiation could allow effective separation of the “wind” component of radiation from the heavy background, which consists of unpulsed radiation of the Crab Nebula at very high (TeV) energies and pulsed radiation at low (GeV) energies. We argue, that even upper limits obtained in such a study could provide unique information about the origin of the pulsar wind.

2 CHARACTERISTICS OF THE WIND

2.1 The total particle ejection rate of the wind

The wind from the Crab pulsar carries away most of the energy of rotation of the pulsar. The energy released in the form of electromagnetic emission of the pulsar, which peaks at gamma-ray energies, does not exceed 1 per cent of the total rotational losses (Arons, 1996), therefore it can be neglected in the energy balance of the wind.

The fluxes of the energy and the angular momentum of the wind consist of two parts. One of them corresponds to the matter and another corresponds to the electromagnetic field. The total flux of the kinetic energy of particles can be presented as

$$\dot{E}_{\text{kin}} = \dot{N}mc^2 \langle \gamma_w \rangle, \quad (1)$$

while the flux of the angular momentum of the matter is equal to

$$\dot{L}_{\text{kin}} = \dot{N}m \langle r\gamma_w v_\varphi \rangle. \quad (2)$$

Here \dot{N} is the total rate of particle ejection from the pulsar magnetosphere, $\langle \gamma_w \rangle$ is the average Lorentz-factor of the wind, r is the distance to the axis of rotation v_φ is the component of the velocity of plasma propagation in the direction of rotation. Hereafter we assume that the wind consists of

only electrons and positrons. The total rate of particle ejection can be estimated within the models e^\pm pair production in the pulsar magnetosphere:

$$\dot{N}_{\text{gap}} = n_\pm c S_{\text{cap}} \lambda, \quad (3)$$

where $S_{\text{cap}} = 2\pi R_*^3 \Omega / c$ is the total area of the polar caps of the neutron star where the roots of the open magnetic field lines are placed, n_\pm is the density of the particles in the primary beam, Ω is the angular velocity of rotation of the pulsar, R_* is the radius of the pulsar and the factor λ takes into account the multiplication of particles because the development of electromagnetic cascades in the magnetosphere. In the inner gap models, the electromagnetic cascade is initiated by a beam of electrons accelerated up to the Lorentz-factor $\gamma_{\text{gap}} \sim 2 \cdot 10^7$ (Ruderman & Sutherland 1975; Arons 1983). The density of particles in the beam is of the order of Goldreich-Julian density $n_\pm = n_{\text{GJ}}$ (Goldreich & Julian 1969) determined as

$$n_{\text{GJ}} = \frac{(\Omega B)}{2\pi ec}. \quad (4)$$

Owing to the electromagnetic cascade in the pulsar magnetosphere, the number of particles increases by a factor of λ and, correspondingly the Lorentz-factor of particles decreases by the same factor.

The calculations by Daugherty & Harding (1982) and Gurevich & Istomin (1985) show that for the Crab pulsar this factor is of order of 10^4 . Note that these early calculations took into account only multiplication resulting from the cascades supported by two processes – the curvature radiation of electrons and e^\pm pair production of γ -rays of these photons in the magnetic field. Meanwhile, the process of the Compton scattering of electrons on the soft thermal emission of the neutron star plays, most probably, a non-negligible role in the cascade development (Arons 1998), thus this effect should be taken into account in the estimates of λ . In any case, the uncertainties in the model parameters and assumptions does not allow an accurate theoretical estimate of λ , but instead give a broad range of possible values of λ between 10^3 and 10^5 . Remarkably, a rather accurate estimate of $\langle \gamma_w \rangle$ in the upstream flow can be derived from the analysis of the nonthermal high energy radiation of the downstream region. Indeed, the explanation of the spectrum of synchrotron X-ray emission by the wind electrons accelerated (redistributed) by the termination shock requires a power-law injection spectrum of the electrons $Q(E) \propto E^{-\alpha}$ with $\alpha \simeq 2.4$ and a cutoff of the spectrum below $E_* \sim 150 - 200$ GeV. Also, the interpretation of the X-ray and TeV γ -ray emissions within the synchro-Compton model of the Crab Nebula allows one to derive, with very good accuracy, the average magnetic field in the downstream region and the total luminosity in shock-accelerated electrons, $B \simeq 2 \cdot 10^{-4}$ G, and $\dot{W} \simeq 3 \times 10^{38}$ erg/s (for review see Aharonian & Atoyan (1998)). The obvious conservation laws concerning both the number and the total energy of the of relativistic electrons in the downstream and upstream regions (i.e. before and after the shock acceleration) gives $\langle \gamma_w \rangle = \frac{\alpha-1}{\alpha-2} (E_*/m_e c^2) \simeq 1.3 \cdot 10^6$. The accuracy of this estimate depends on the possible range of variation of the parameters α and E_* that still fit the data, and is estimated smaller than factor of 4. Correspondingly we find the injection rate of the wind particles

$\dot{N} = \dot{W} / \langle \gamma_w \rangle m_e c^2 = 2.8 \cdot 10^{38} \text{ s}^{-1}$. This implies that for $\dot{N}_{\text{gap}} = 2 \cdot 10^{34}$ the λ -factor should be close to 10^4 .

Thus, the cascade multiplication of the primary electrons accelerated in the pulsar magnetosphere leads to the formation of an e^\pm plasma with parameters

$$\dot{N} = \frac{\lambda B_0 \Omega^2 R_*^3}{ec^2}, \quad (5)$$

and

$$\gamma_{w0} = \frac{\gamma_{\text{gap}}}{\lambda}. \quad (6)$$

The Lorentz factor of this initial wind is close to $\gamma_{w0} \sim 10^3$ while the kinetic energy flux of the wind is

$$\dot{E}_0 \approx \gamma_{w0} m c^2 \dot{N} \quad (7)$$

For the Crab pulsar this flux is estimated as $1.6 \times 10^{35} \text{ erg/s}$. It is much lower than the total rotational losses of the pulsar $\dot{E}_{\text{rot}} = 4 \times 10^{38} \text{ erg/s}$ (see e.g. Shklovsky (1968)). This leads to a conclusion that the most part of pulsar's rotational energy is carried off by the electromagnetic field (see e.g. Arons (1996)). The state of the wind is characterized by so-called σ -parameter determined as the ratio of the electromagnetic energy flux to the kinetic energy flux of particles in the wind. At $\sigma_w \geq 1$ the wind is Poynting-flux dominated. At $\sigma_w \leq 1$ the wind is kinetic-energy-dominated. Initially the wind ejected from the pulsar magnetosphere is Poynting flux dominated, because $\sigma_{w0} = \dot{E}_{\text{rot}} / \dot{E}_0 \sim 2.5 \cdot 10^3$. The estimates of the wind parameters in the outer gap model gives essentially the same magnetization parameter (Cheung & Cheng 1994; Coroniti 1990).

On the other hand, the explanation of the characteristics of the nonthermal radiation of the Crab Nebula requires that σ_w be between 10^{-3} and 10^{-2} in the wind region upstream of the termination shock (Rees & Gunn 1974; Kennel & Coroniti 1984). Thus the magnetization parameter σ_w decreases by several orders of magnitude on the way from the light cylinder to the pre-shock region. Therefore it is difficult to avoid a conclusion that the wind is additionally accelerated in a some region beyond the light cylinder.

The theory by Kennel & Coroniti (1984) is based on the assumption of ideal MHD flow of the plasma after the terminating shock wave. All dissipative processes are neglected, with exception of the cooling of the plasma due to the synchrotron emission. Lyubarskii (1992) and Begelman (1998) argued that the theory of Kennel & Coroniti (1984) is likely not complete. The magnetic field after the terminating shock is mainly toroidal. It is very well known in plasma physics that such configuration is strongly unstable (Bateman 1980). The instabilities can essentially change the physics of the flow in the Nebula. The basic process is the fast dissipation of the toroidal magnetic field with conversion of its energy into the energy of the relativistic particles. The instability drives the plasma towards equipartition of energy between the magnetic field and the matter. This process will inevitably be accompanied by acceleration of particles. The dissipative processes provide the dynamics of the plasma, in good agreement with the observed velocity of the expansion of the outer edge of the nebula, even for the parameter $\sigma_w \sim 1$. We emphasize that, although very reasonable, this argument nevertheless does not solve the problem of the wind acceleration, because even in this case we have to transform wind with $\sigma_{w0} \sim 10^3$ into wind with

$\sigma_w \sim 1$. Moreover, the wind with $\sigma_w \sim 1$ has almost the same characteristics as we presented above. The only exception is that the Lorentz factor of the wind with $\sigma_w \sim 1$ is twice as small as that of the wind with $\sigma_w \sim 10^{-3}$. In the limits of uncertainty of the multiplication factor λ this difference is not important, however

2.2 The energy spectrum of the wind electrons

Here we assume that the wind with $\sigma \ll 1$ is formed in some 'acceleration region' at a distance to the axis of rotation R_w . We also assume that the plasma axially isotropically fills all the open field lines. Thus, the wind is not modulated in the azimuthal direction.

For calculation of the spectra of emission we need information about spatial and energetic distribution of particles of the wind. Let us first summarize the information about these characteristics following directly from observations. The average Lorentz-factor of the wind in the regime of $\sigma \leq 1$ is determined as

$$\langle \gamma_w \rangle = \frac{\dot{E}_{\text{rot}}}{\dot{N}}, \quad (8)$$

with a typical value $\sim 10^6$.

The kinetic-energy-dominated wind is believed to be cold, because the region of the flow of this wind is observed as an 'underluminous' region (see Kennel & Coroniti (1984) and referenced literature). Otherwise, a hot wind would produce remarkable synchrotron emission, which would contradict the existence of underluminous region.

There is definite latitudinal inhomogeneity of the wind. The observations by ROSAT of the torus of X-ray emission in the Crab Nebula clearly demonstrate that energy flux in the wind varies with latitude (Hester et al. 1995). This fact means that the density of the wind, its Lorentz-factor and the toroidal magnetic field should depend on the latitude.

It is believed that the existence of an X-ray torus implies that the wind flows predominantly in narrow disc-like sector along the equator with opening angle less than 30° (Hester et al. 1995). However, one should take into account the fact that optical emission is uniformly distributed in the Nebula. This means that there should be a component of the wind at high latitudes. As the luminosities in optical and in X-rays are comparable the energetics of this high latitude wind component is comparable with the energetics of the equatorial component which produces the X-ray torus. Moreover, the evidence that the wind at high latitudes exists close to the pulsar follows also from HST observations (Hester et al. 1995). In our calculations we assume that the particle flux in the wind is isotropic. However to be consistent with observations in X-rays we assume that the Lorentz-factor and the toroidal magnetic field of the wind depend on latitude.

There are no model independent estimates of the latitudinal dependence of the Lorentz-factor of the wind and toroidal magnetic field. We use here the characteristics of the wind obtained in the model of an axisymmetric rotator (Bogovalov 1997). These characteristics are also valid for oblique rotators (Bogovalov 1999).

Below we assume that

$$\gamma_w = \gamma_{w0} + \gamma_{\text{max}} \cos^2(\alpha), \quad (9)$$

where $\gamma_{\text{max}} = \sigma_{w0} \gamma_0$ is the maximum Lorentz-factor of the

plasma on the equator ($\alpha = 0$); $\gamma_0 \sim 10^3$ (see equation 6) and $\sigma_{w0} \sim 10^3$ are the Lorentz-factor and the magnetization parameter of the wind near the light cylinder. The wind is assumed to be monoenergetic at a given latitude. It follows from equation (9) that

$$\langle \gamma_w \rangle = \frac{2}{3} \gamma_{max}. \quad (10)$$

In the particular case of the axisymmetric rotator (Bogovalov & Kotov 1992),

$$\gamma_{max} = \frac{eB_0 R_*}{2mc^2 \lambda} (R_* \Omega / c)^2. \quad (11)$$

2.3 The geometry of the wind flow

The geometry of the flow and of the IC process are drawn in fig. 1. The neutron star is placed on the axis of rotation and ejects the wind radially. The dash-dotted vertical lines show the light cylinder. The wind is accelerated in the acceleration zone by some unspecified mechanism and at the distance R_W it has characteristics discussed above. The acceleration is completed at R_W . Beyond R_W particles in the wind move along straight lines without further acceleration. The equatorial plane of the pulsar is inclined in relation to the observer at the angle $\alpha = 33^\circ$ (Hester et al. 1995). IC photons move along the direction of motion of electrons. Therefore only the particles of the wind directed towards Earth can produce observable emission. The lines of flow of the cold kinetic energy dominated wind after acceleration are not exactly radial. Classical mechanics provides a simple relationship between the rates of the rotational energy losses of the pulsar, $\dot{E}_{rot} = I\Omega\dot{\Omega}$, and the angular momentum losses, $\dot{L} = I\dot{\Omega}$:

$$\dot{E}_{rot} = \dot{L}\Omega. \quad (12)$$

Here I is the momentum of inertia of the neutron star. As the electromagnetic field carries off practically no energy in the kinetic-energy-dominated wind, it does not carry the angular momentum either. In the theory of plasma flow in the magnetosphere of an axisymmetric rotator this statement is verified immediately (Bogovalov 1997). Under this condition it follows from equations (1), (2), and (12) that after the acceleration the azimuthal velocity of the wind v_φ is connected with R_W as

$$\frac{v_\varphi}{c} = \frac{R_L}{R_W}. \quad (13)$$

From this relationship and from Fig. 1 it follows that the projection of the vector of the velocity of the plasma after acceleration lies on the line tangential to the light cylinder. The angle θ between the direction of the motion of relativistic particles in the wind and the soft thermal photons emitted from the pulsar depends on distance r to the axis of rotation:

$$\sin \theta = \cos \alpha \frac{R_L}{r}. \quad (14)$$

It is seen from this relationship that at any distance from the pulsar there is a non-zero angle between the radial direction and the velocity of the wind. The Inverse Compton scattering of the wind electrons on soft photons emitted as a fan-like beam from the inner magnetosphere of the pulsar results in the production of hard γ -ray photons. Equations

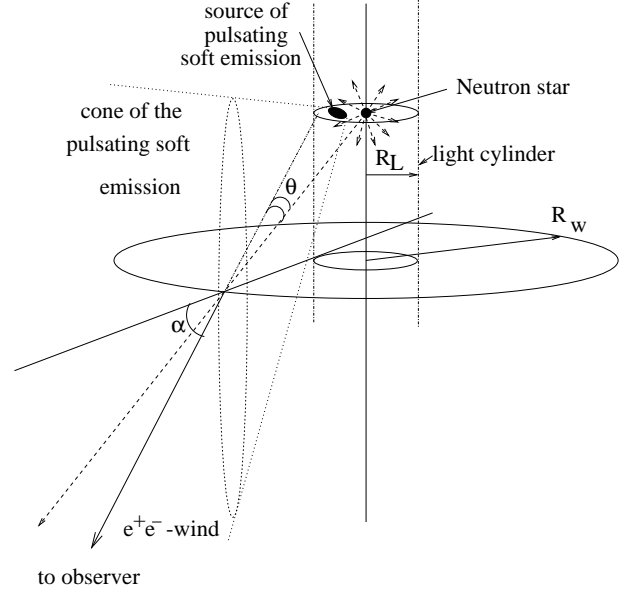


Figure 1. A sketch of the trajectories of plasma after acceleration, and the assumed position of sources of soft photons.

(14) and (13) remain valid for condition $\gamma_w \gg \gamma_{w0}$ (Bogovalov 1997), also fulfilled in the wind with $\sigma_w \sim 1$. Below we will not distinguish between the cases with $\sigma_w \ll 1$ and $\sigma_w \sim 1$.

The angular distribution of soft emission close to the pulsar is not well known. In the outer gap model the optical and soft x-ray emission is generated inside, but not far from the light cylinder (Romani & Yadigaroglu 1995). There are several sources of soft emission in the magnetosphere corresponding to the position of the outer gaps. In this model, the projection of the motion of photons from these sources on the equatorial plane is predominantly directed radially. Then the angle between direction of motion of the wind and soft non-thermal photons can also be estimated by equation (14). Note that at $R_W \gg R_L$ the IC flux does not depend on the position of the source inside the magnetosphere if the soft photons are emitted radially.

Our calculations of IC radiation are based on the assumption that the wind is illuminated only by the emission that is directed to Earth. However, as we can not exclude the existence of an additional component of optical emission not directed to the observer, but illuminating the wind, our estimates of γ -ray flux could be considered only as a lower limit.

3 INVERSE COMPTON RADIATION OF THE WIND

3.1 The fields of soft photons

The soft emission from the Crab pulsar consists of two, pulsed and unpulsed, components. The recent ROSAT observations allowed one to distinguish the contribution of the pulsar in the observed unpulsed flux from the emission of the nebula. The main contribution to the unpulsed radiation of the pulsar comes, most probably, from the thermal emission of the hot surface of the neutron star. According

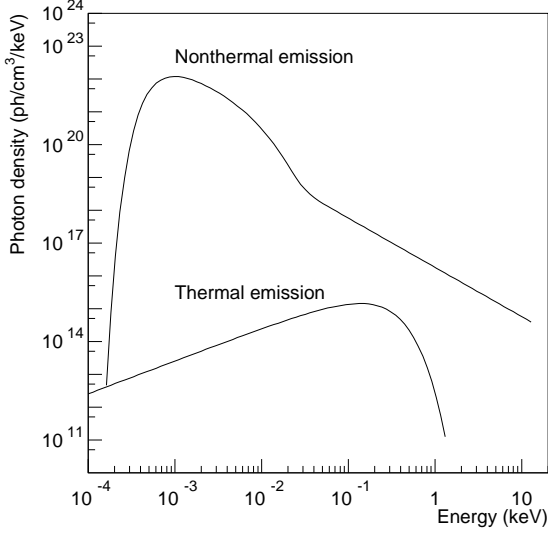


Figure 2. The averaged spectral density of photons near the light cylinder of the Crab pulsar

to the ROSAT observations, the total energy flux of the unpulsed emission in the range 0.1 - 2.4 keV is 10^{34} erg/s (Becker & Trümper 1997). The latter could be approximated by black-body spectrum with a temperature $1.9 \cdot 10^6$ K and total luminosity 10^{34} erg/s.

The pulsed soft radiation of the pulsar is dominated by nonthermal processes in the magnetosphere. The photons in the optical to X-ray band of this radiation play the most important role in the production of inverse Compton γ -rays. Measurements of the spectra of the pulsed optical emission by different groups (Nasuti et al. 1996; Oke 1969; Percival et.al. 1993) give the following spectra of optical photons in the range 1680 - 7400 Å

$$F_\nu = 3.1 \left(\frac{\nu}{\nu_0}\right)^{-0.11} \text{ mJy}, \quad (15)$$

where $\nu_0 = 6.82 \cdot 10^{14}$ Hz.

The X-ray data in the range of 0.1 - 2.4 keV obtained by ROSAT can be approximated by a power-law with the photon index 1.5 and luminosity (assuming that the radiation is emitted isotropically) $7.1 \cdot 10^{35}$ erg/s (Becker & Trümper 1997).

The extrapolation of the soft x-ray emission spectrum to the optical range gives lower flux than is observed (Knight 1984). This means that the optical emission has a cutoff in the ultraviolet region. Unfortunately there are no data for the pulsating emission in this region. Therefore we assume an exponential cutoff in the spectrum above 0.05 keV. The emission is also strongly suppressed at infrared wavelengths (Middleditch et al. 1983). Below we use the following approximation of the averaged density of non-thermal photons near the light cylinder

$$n(\epsilon) = Z(\epsilon) \exp \left[- \left(\frac{8 \cdot 10^{-4} \text{ keV}}{\epsilon} \right)^2 \right] \cdot \frac{\text{photon}}{\text{cm}^3 \text{keV}}, \quad (16)$$

where ϵ is the energy of photons in keV and

$$Z(\epsilon) = 1.82 \cdot 10^{16} \epsilon^{-1.5} +$$

$$+ 1.25 \cdot 10^{19} \epsilon^{-1.11} \exp \left[- \left(\frac{\epsilon}{5 \cdot 10^{-3} \text{ keV}} \right) \right] \frac{\text{ph}}{\text{cm}^3 \text{keV}} \quad (17)$$

The photon density of thermal and non-thermal components of low-frequency radiation on the light cylinder is shown in Fig. 2. We assume that the density of the both photon fields fall off with distance to the pulsar center R as $1/R^2$.

3.2 The fluxes and spectra of gamma radiation

The optical depth characterizing the Compton scattering of the wind electrons propagating through the radiation fields of the pulsar is defined as

$$\tau = \int \sigma(\omega, \gamma, \mathbf{v}, \mathbf{c}) (1 - \mathbf{v}\mathbf{c}) n_{ph}(\omega, \mathbf{c}, r) dl d\omega, \quad (18)$$

where $\sigma(\omega, \gamma, \mathbf{v}, \mathbf{c})$ is the total invariant cross-section of the IC scattering, ω is the energy of soft photons in mc^2 . Integration of equation (18) over dl is performed along the trajectory of a wind electron (see Fig. 1) from the wind formation position to infinity.

The γ -ray energy flux at the angle α to the plane of the pulsar equator is equal to

$$L_{IC}(E_\gamma) = \frac{\dot{N}}{4\pi D^2} \times \int \int E_\gamma \frac{d\sigma}{dE_\gamma}(\gamma_w(\alpha), \omega, E_\gamma, \theta) n_{ph}(\omega, \mathbf{c}, \mathbf{r}) d\omega dl, \quad (19)$$

where $D = 2$ kpc is the distance to the source, $\frac{d\sigma}{dE_\gamma}(\gamma_w(\xi), \omega, E_\gamma, \theta)$ is the differential cross-section of the Compton scattering of a photon with energy ω and electron with γ_w encountering under angle θ and producing a photon with energy E_γ . This cross-section was obtained after integration of the differential cross-section (Berestetskii, Lifshitz & Pitaevskii 1971) over the emission angle

$$\frac{d\sigma}{dE_\gamma}(\gamma, \omega, E_\gamma, \theta) = \frac{\pi r_e^2}{(pk)^2} \left\{ \frac{1}{(pk)^2} - \frac{2I}{(pk)\gamma_c\omega_c} + \frac{I^3(1-U\delta\beta)}{(\gamma_c\omega_c)^2} + 2\left(\frac{1}{(pk)} - \frac{I}{\gamma_c\omega_c}\right) + \left(\frac{(pk)I}{\gamma_c\omega_c} + \frac{\gamma_c\omega_c(1-U\delta\beta)}{(pk)}\right) \frac{\omega_c}{\Gamma V_c} \right\}, \quad (20)$$

where

$$(pk) = \gamma\omega(1 - v \cos \theta), \quad V_c = \frac{\sqrt{\omega^2 + (\gamma v)^2 + 2\gamma v \omega \cos(\theta)}}{(\gamma + \omega)},$$

$$\Gamma = \frac{\gamma + \omega}{\sqrt{1 + 2(pk)}}, \quad \omega_c = \frac{(pk)}{\sqrt{1 + 2(pk)}},$$

$$\gamma_c = \frac{1 + (pk)}{\sqrt{1 + 2(pk)}}, \quad U = \frac{(pk)}{1 + (pk)},$$

$$\delta = \frac{1}{V_c} \left(\frac{E_\gamma}{\Gamma \omega_c} - 1 \right), \quad \beta = \frac{1}{UV_c} \left(\frac{\gamma}{\Gamma \gamma_c} - 1 \right).$$

Function I in equation (20) is defined as follows

$$I = (1 - U^2 - 2U(1 - U)\beta\delta + U^2(\delta - \beta)^2)^{-1/2}. \quad (21)$$

Integration of equation (19) is performed along the trajectory of a electron and over the spectra of soft photons. It is assumed that the observer detects photons from a monoenergetic beam of electrons from the wind moving to the observer. We take $\gamma_{\max} = \frac{3}{2} \dot{E}_{\text{rot}} / \dot{N}$, with $\gamma_w(\alpha) =$

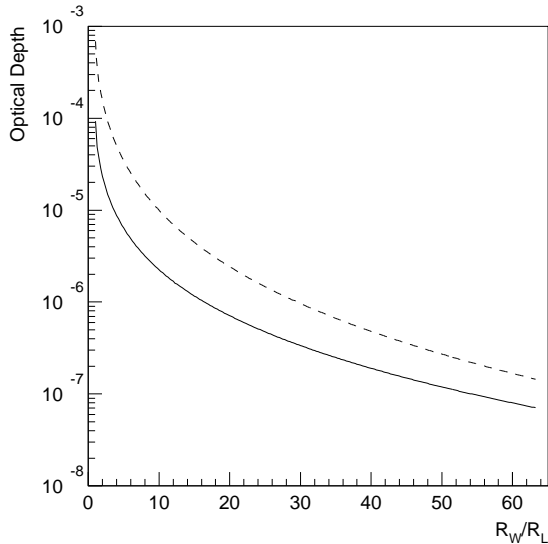


Figure 3. The optical depth of the thermal photon field for the IC scattering of electrons with Lorentz factor $\gamma_w = 4 \cdot 10^6$ (dashed line) and $4 \cdot 10^7$ (solid line).

$\gamma_{\max} \cos^2(33^\circ)$, since the plane of the pulsar equator is inclined to the observer at the angle 33° (Hester et al. 1995).

3.3 IC photons from thermal isotropic radiation

The optical depth τ , and therefore the spectra of IC photons, depends strongly on the distance R_w at which the kinetic energy dominated wind is formed.

The dependence of the optical depth on R_w is shown in Fig. 3 for two different values of the Lorentz factors of the wind $\gamma_w = 4 \cdot 10^6$ and $4 \cdot 10^7$. Strong dependence of τ on γ_w is explained by the fact that the optical depth is dominated by IC scattering at small distances from the pulsar where $2\omega\gamma(1 - \cos(\theta)) \gg 1$, i.e. the Compton scattering takes place in the Klein-Nishina regime. In this regime the IC cross-section decreases with the electron energy as γ_w^{-1} , which lead to larger optical depth for smaller values of the Lorentz-factor of the wind γ_w . This effect is especially strong for small values of R_w . In this case the optical depth is accumulated by IC scattering close to the light cylinder where the collision angle θ is large, and the IC scattering takes place in deep Klein-Nishina regime.

In many ‘‘standard’’ astrophysical situations the efficiency of the γ -ray production in the Klein-Nishina regime is significantly suppressed because of the synchrotron cooling of electrons. In the case of a *cold* wind we deal with a unique situation when the synchrotron losses of electrons are completely suppressed, and thus the wind electrons lose their energy only through the inverse Compton radiation. Note that in deep Klein-Nishina regime, namely when $2\gamma_w\omega(1 - \cos\theta) \geq 10^4$, the triplet pair production dominates over the inverse Compton scattering (Mastichiadis 1991; Dermer & Schlickeiser 1991). This process results in production of new electrons. However, as in all interesting cases the optical depth $\tau \leq 1$, the secondary electrons do not increase significantly the density of the wind. Therefore

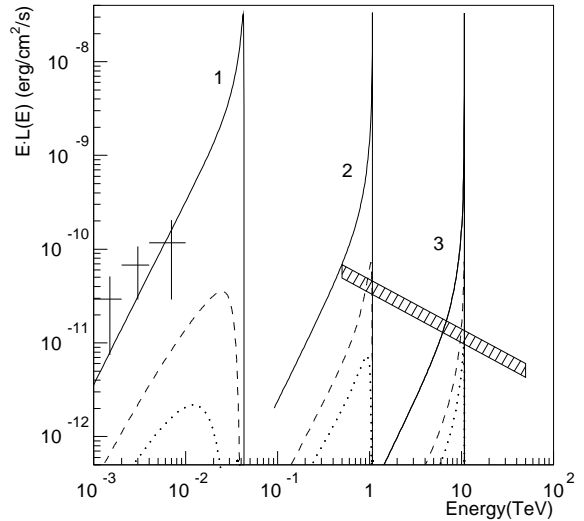


Figure 4. The spectra of IC radiation of the wind illuminated by the thermal emission of the pulsar. It is assumed that the kinetic-energy-dominated wind is formed at distances of 1 (solid), 5 (dashed), and 10 (dotted) light cylinders from the pulsar. The curves 1,2,3 correspond to $\gamma_{\max} = 1.2 \cdot 10^5, 3 \cdot 10^6, 3 \cdot 10^7$. The range of observed fluxes of γ -rays in the region above 500 GeV detected by CAT, CANGAROO, HEGRA and Whipple telescopes is shown by a shadowed region. The points with error bars below 10 GeV correspond to the unpulsed fluxes measured by EGRET.

we ignore this process here. The same is true also for another process connected with absorption of TeV γ -rays in the magnetic field of the wind (see Appendix).

In fig. 4 we present the expected γ -ray fluxes of the wind. Solid, dashed and dotted lines correspond to the fluxes produced by a wind originated at $R_w/R_L=1, 5$ and 10 . Remarkably, the spectrum of IC γ -rays has a specific line feature since the radiation is produced in the Klein-Nishina regime. Because of this feature, the IC radiation of the wind can be easily distinguished from the smooth spectra of the Crab Nebula. The corresponding integral fluxes are shown in Fig. 5 for different γ_w and R_w .

The comparison of the calculated spectra with the observed TeV γ -ray fluxes of the Crab Nebula (for review see Weekes et al. 1997) leads to an interesting conclusion that for any reasonable Lorentz-factor of the wind, the calculated γ -ray fluxes significantly exceed the observed fluxes unless the wind is formed well beyond the light cylinder. This implies a meaningful constraint on the ‘birthplace’ of the kinetic energy dominated wind with $\gamma_w \geq 10^6$: $R_w \geq 5R_L$. For $\gamma \leq 1.2 \cdot 10^5$, a similar conclusion is imposed by the EGRET (Nolan et al. 1993) observations of unpulsed radiation above 1 GeV. The lack of measurements in the energy region between 10 GeV and 300 GeV does not completely exclude a possibility of formation of the particle dominated wind close to the light cylinder, if one assumes that $10^5 < \gamma_{\max} < 10^6$. Although the analysis of the observed synchrotron and IC components of the nonthermal radiation of the Crab Nebula gives certain preference to larger wind Lorentz factors, $\gamma_w \sim 10^6$, it is important to have *observational* constraints on R_w also for γ_w in the region between 10^5 to 10^6 , which is

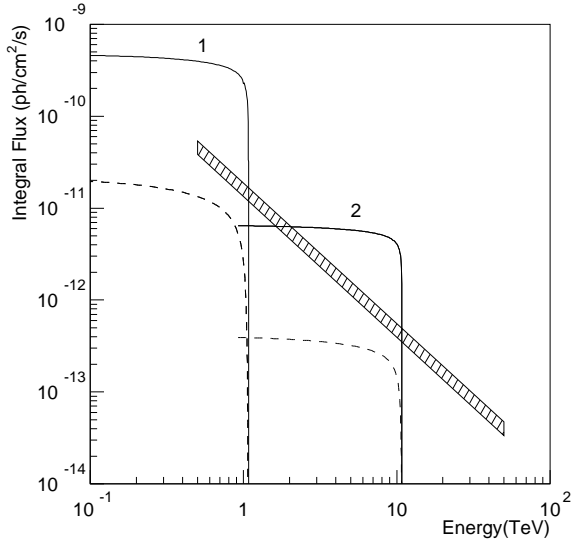


Figure 5. The integral fluxes of IC radiation of the wind illuminated by the thermal emission of the pulsar. It is assumed that the kinetic-energy-dominated wind is formed at distances of 1 (solid line) and 5 (dashed line) light cylinders from the pulsar. The curves 1 and 2 correspond to $\gamma_{max} = 3 \cdot 10^6$ and $3 \cdot 10^7$ respectively. The range of observed fluxes of γ -rays in the region above 500 GeV is shown by a shadowed region.

presently missing This should be provided in the near future by measurements of the Crab spectrum between 10 and 300 GeV by the new generation of low-threshold atmospheric Cherenkov detectors as well as by the GLAST.

3.4 The interaction of the wind with the nonthermal emission

The IC γ radiation caused by illumination of the wind by pulsed soft photon emission should be modulated at the same pulsation period. This conclusion is true even for the isotropic wind. For calculation of the IC fluxes it is assumed that the nonthermal source of soft emission is located inside the light cylinder (see Fig. 1). It is easy to show that under realistic conditions the phase curve of the gamma-rays should be close to the phase curve of the soft emission. Indeed, let us assume for simplicity that the beam is very narrow (delta-function like). Owing to the rotation of the pulsar, it will form a spiral. The point where this spiral crosses the line tangential to the light cylinder and directed towards the observer is the source of γ -rays (see Fig. 6). The width of the γ -ray pulse is determined by the delay in the arrival time δt of optical and gamma-ray emission to the observer:

$$\delta t \sim \frac{\theta T}{2\pi}, \quad (22)$$

where θ is the maximal value of the angle between the wavevector of photons and the velocity of the particles in the wind, T is the period of rotation. In the most interesting case, $\theta \ll 1$, the phase curves of gamma-ray emission produced in the process under consideration and those of the optical emission illuminating the wind are expected to be

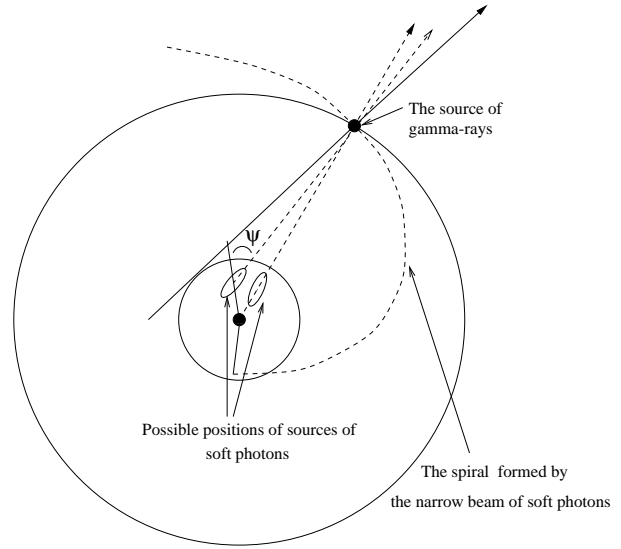


Figure 6. The angle between the wavevector of soft photon and the velocity of particles in the wind depends on the position of the source of soft photons inside the magnetosphere and the direction of the beam. The minimum efficiency of the gamma-ray production is achieved when the source is corotating with the pulsar. The narrow beam of non-thermal soft photons produces a spiral in space. The point of crossing of this spiral with the trajectory of an electron moving to an observer is the source of γ -ray photons, which moves with a velocity very close to the light velocity. At small angles between the beam of the soft photons and the velocity of particles in the wind, the delay in the arrival time of hard photons and optical photons is small. The width of the gamma-ray pulse is also small. The phase curves for optical radiation illuminating the wind and in VHE gamma-rays are expected to be similar.

similar. However, because we observe only the pulsed soft emission directed to us and do not observe other possible part of the emission (not directed towards the observer) that can illuminate the wind, there could be a difference between the γ -ray and directly observed soft emission light curves.

It is seen from Fig. 2 that the average density of non-thermal photons is several orders of magnitude larger than the density of the thermal photons. Therefore, the IC optical depth for an electron is much larger than in the case of thermal radiation (see Fig.7). In particular, at $R_W \leq 5R_L$ the optical depth $\tau \geq 1$. As the IC scattering takes place in the Klein-Nishina regime, one or two interactions are sufficient to destroy the wind, and the whole energy of the wind electrons would be transferred to γ ray emission with huge luminosity $\geq 10^{38}$ erg/s. This very fact excludes the possibility of formation of the kinetic dominated wind within $5R_L$. Moreover, this conclusion can be extended to larger distances. Fig. 8 shows the spectra of the emission for two maximal energies of the electrons in the wind. Solid lines show the spectra for $\gamma_{max} = 3 \cdot 10^6$ and dashed lines show the spectra for $\gamma_{max} = 3 \cdot 10^7$. In contrast to the IC γ -rays from interaction with thermal emission, there are no lines in the spectra of the emission because the IC scattering takes place in the Thomson regime. The spectra consist of two well separated broad components, corresponding to two components in the spectra of the soft nonthermal emission presented in Fig. 2. The comparison of calculated γ -ray

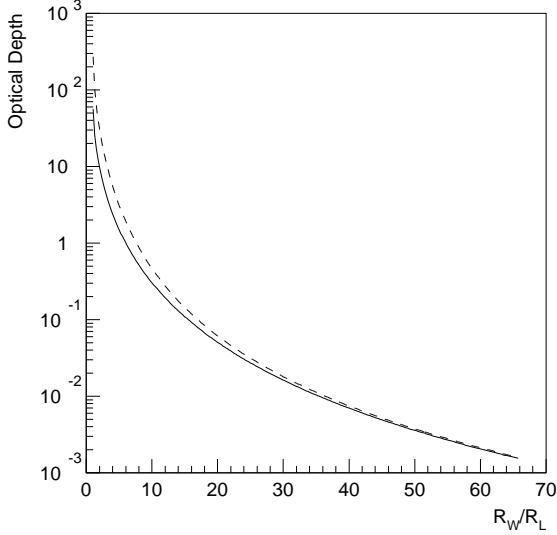


Figure 7. The optical depth for IC scattering of electrons on nonthermal pulsating radiation of the pulsar. It is assumed that the nonthermal photons are directed radially. Curves are given for $\gamma_w = 4 \cdot 10^6$ (dashed line) and for $\gamma_w = 4 \cdot 10^7$ (solid line).

fluxes with upper limits on pulsed emission reported by the Whipple (Weekes et al. 1998) and HEGRA (Aharonian et al. 1999) groups shows that the wind must be formed at relatively large distances from the pulsar, $R_W > 30R_L$.

The spectra shown in Fig. 8 were calculated at the assumption that the nonthermal source emits photons along the radial direction from the pulsar as it happens in the outer gap model (Romani & Yadigaroglu 1995). Self-consistent MHD solutions confirm that the plasma should move predominantly radially in the pulsar magnetosphere (Bogovalov 1997). Therefore the source of nonthermal photons should indeed emit along the radial direction from the pulsar. In the model by Lyubarskii (1996) the source of the soft nonthermal photons emits in the direction opposite to the direction of rotation of the pulsar. If so, the γ -ray emission would be even higher than shown in Fig. 4.

We are not aware of models in which the source of photons corotates with the pulsar and emits photons tangentially along the direction of rotation. In this case the angle of interaction θ is minimum and correspondently the IC flux is expected to be reduced. Although it is almost unlikely that the plasma (and source of soft photons) can corotate with the pulsar, it is perhaps wise to consider this limiting case from pedagogical point of view in some detail.

Optical and soft X-ray emission can be produced by plasma moving with a Lorentz-factor of order $\gamma_e \sim 10^2 - 10^3$ in the pulsar magnetosphere. At corotation with the pulsar the plasma have azimuthal velocity $v_\varphi = \frac{r\Omega}{c}$, where r is the radius in the cylindrical system of coordinates. Since these particles should also be directed towards the observer, they have the component of the velocity $v_z = c \cos \alpha$. From the relativistic relationship it follows that

$$\gamma_e^2 = 1 + \gamma_e^2 [\cos^2 \alpha + (\frac{r_s \Omega}{c})^2 + (\frac{v_r}{c})^2], \quad (23)$$

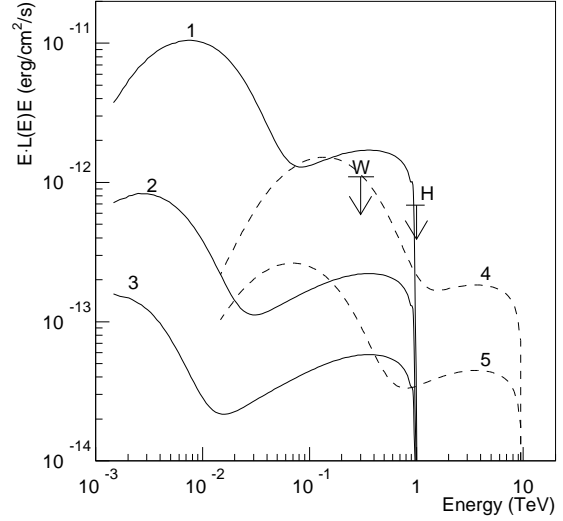


Figure 8. The spectra of pulsating TeV gamma-ray emission produced by the wind with $\gamma_{max} = 3 \cdot 10^6$ (solid lines) and $\gamma_{max} = 3 \cdot 10^7$ (dashed lines). Numbers 1, 2 and 3 near the solid lines correspond to $R_w/R_L = 30, 50$ and 70 , respectively. The curves 4 and 5 correspond to $R_w/R_L = 70$ and 100 . The upper limits on the pulsed radiation from Crab Nebula above 300 GeV given by Whipple group (Weekes et al. 1998) and above 1 TeV given by HEGRA collaboration (Aharonian et al. 1999) are also shown. The beam of soft photons is assumed to be radial.

where r_s is the distance from the source to the center of the pulsar, v_r is the radial component of the velocity. The soft photons are emitted at the angle ψ as shown in Fig. 6. Neglecting the term $1/\gamma_e^2$ we obtain that

$$\sin \psi = \frac{r_s \Omega}{c \sin \alpha}. \quad (24)$$

This relationship shows that a source that emits soft photons in direction to the observer and corotating with the pulsar can not be located exactly on the light cylinder.

Fig. 9 demonstrates how the spectra of IC radiation depend on the position of the corotating source of the soft photons inside the pulsar magnetosphere for parameters of the kinetic energy dominated wind at $R_w = 40R_L$. Curve 1 corresponds to the emission from the corotating source located on the surface of the pulsar. The same flux is produced by the source of soft photons with the beam directed radially from the pulsar; the IC flux generated from the last source does not depend on r_s . Therefore comparison of the curve 1 with others allows one to compare the fluxes of IC photons produced at the scattering of electrons on the soft emission from the corotating source and the source with the soft photons emitted radially, but located on the same distance r_s . It follows from this figure that the flux of the IC photons can be reduced to zero only at the position of the source of soft photons not far from the light cylinder. At any other position of the source the efficiency of generation remains high at $r_s < 0.6R_L$. The existing upper limit on the pulsating flux from the Crab pulsar means that either the wind is formed beyond $30R_L$ or the wind is formed close to the light cylinder but the pulsating source of soft nonther-

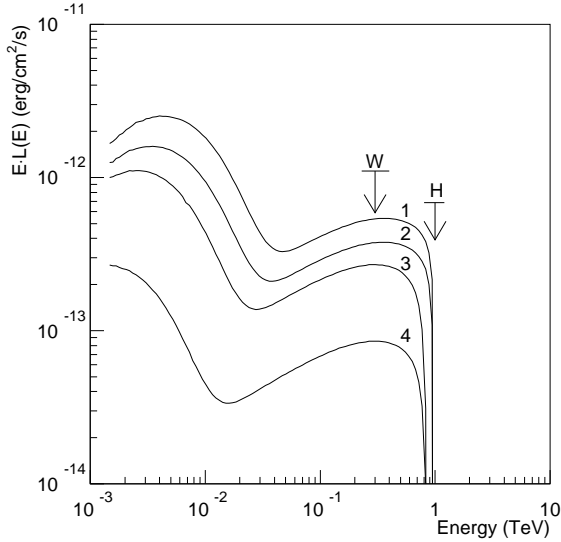


Figure 9. The dependence of the differential spectra of γ -ray emission on the position of the source of soft photons inside the pulsar magnetosphere for parameters of the wind $\gamma_{max} = 3 \cdot 10^6$ at $R_W = 40R_L$. The source of soft photons is placed on the distance $r_s = 0., 0.3, 0.5, 0.6R_L$ respectively for curves 1, 2, 3, 4. The direction of the beam of the soft photons was defined under the assumption of corotation of emitting particles with the pulsar.

mal photons corotates with the pulsar and is located close to the light cylinder.

4 SUMMARY

The Crab Nebula is a unique cosmic laboratory with an unprecedentedly broad spectrum of the observed nonthermal radiation that extends throughout 21 decades of frequency – from radio wavelengths to very high energy γ -rays (for review see e.g. Aharonian & Atoyan 1998) It is commonly accepted that the synchrotron nebula is powered by the relativistic wind of electrons generated at the pulsar and terminated by a standing reverse shock wave at a distance $r_s \sim 0.1$ pc (Rees & Gunn 1974). The relativistic MHD models, even in their simplified form (e.g. ignoring the axisymmetric structure of the wind and its interaction with the optical filaments), successfully describe the general characteristics of the synchrotron nebula, and predict realistic distributions of relativistic electrons and magnetic field in the downstream region behind the shock (Kennel & Coroniti 1984). Meanwhile our knowledge of the unshocked wind, i.e. about the region between the pulsar magnetosphere and the shock is based only on theoretical speculations. Moreover, it is commonly thought that the wind could not be visible in the region upstream of the termination shock because the relativistic electrons and magnetic field in wind move together, thus the unshocked wind does not produce synchrotron radiation. In this paper we show that the kinetic energy dominated wind nevertheless could be directly observed through its IC radiation because of the illumination of the wind by low-energy radiation of the pulsar. The γ -ray emission consists of two components, pulsed and unpulsed,

associated with the nonthermal and thermal low-energy radiation components of the pulsar, respectively.

The unpulsed component of γ -ray emission associated with thermal radiation of the pulsar with temperature $\simeq 2 \cdot 10^6$ K is produced in deep the Klein-Nishina regime, and therefore has a very sharp (line-like) spectral feature which peaks at energy $E \simeq \gamma_w m_e c^2$. Detection of this component would therefore result in unique information about the Lorentz-factor of the bulk motion of the wind. The nonthermal radiation of the pulsar has rather broad energy spectrum which extends to optical and infrared wavelengths, and therefore the IC γ -ray emission associated with this component takes place, to a large extent, in the Thomson regime. This results in a broad γ -ray spectrum with a sharp cutoff at $E \simeq \gamma_w m_e c^2$.

The absolute γ -ray fluxes of both components depend strongly on the site of formation of the kinetic dominated wind, as well as the Lorentz-factor and the geometry of propagation of the wind. Thus even the flux upper limits of these γ -ray components should provide important constraints on the wind parameters. In particular, we show that the comparison of the calculated flux of the unpulsed inverse IC emission with the measured γ -ray flux of the Crab Nebula excludes the possibility of formation of the kinetic-energy-dominated wind within 5 light cylinder radii of the pulsar, $R_w \geq 5R_L$. The analysis of the pulsed IC emission, calculated under reasonable assumptions concerning the production site and angular distribution of the optical pulsed radiation, yields even tighter restrictions, namely $R_w \geq 30R_L$.

The mechanism of γ -radiation of the wind of the Crab pulsar discussed in this paper should certainly take place in other pulsars as well. However, from the point of view of detection of this radiation, the Crab is a unique object due to its very powerful wind and relatively high luminosity of thermal and nonthermal low-energy radiation, which provides seed photons for the IC scattering. In other pulsars the IC γ -ray fluxes of unshocked winds are expected to be below the detection threshold of current γ -ray instruments, unless the kinetic energy dominated winds of pulsars are produced very close to the light cylinder. The situation could be different in binary systems containing a pulsar and luminous optical companion, the latter being an effective supplier of seed photons for IC scattering. For example, the pulsar/Be star binary system PSR 1259-63 seems to be a unique object for the search for IC TeV radiation from both shocked (Kirk, Ball & Skjæraasen 1999) and unshocked (Kirk & Ball 1999) winds of the pulsar.

Acknowledgments

We thank the Astrophysics group of the MPI für Kernphysik, in particular, H. J. Völk, A.M. Atoyan, J.G. Kirk, as well as L. Ball and Yu. Lyubarskii for many fruitful discussions. SB thanks MPI für Kernphysik for warm hospitality and support during his work on this project.

REFERENCES

- Aharonian F. et al. (HEGRA collaboration), 1999, *A&A*, 346, 913
 Aharonian F.A., Atoyan A.M. 1998, in “Neutron Stars and Pulsars”, Ed. Shibazaki N., Kawai N., Shibata N., Kifune T., Universal Academy Press, p. 339
 Atoyan A.M., Aharonian F.A., 1996, *MNRAS*, 278, 525
 Arons J., 1983, *ApJ*, 266, 215

- Arons J., 1996, *A&A. Suppl. Ser.*, 120, 49
Arons J., 1998, in “Neutron Stars and Pulsars”, Ed. N.Shibazaki, N,Kawai, S.Shibata, T,Kifune. Universal Academy Press, p. 339
Bateman G., 1980, *MHD Instabilities*. Cambridge MIT Press
Becker W., Trümper J., 1997, *A&A*, 326, 682
Begelman M.C., Zhi-Yun Li., 1994, *ApJ*, 426, 269
Begelman M.C., 1998, *ApJ*, 493, 291
Berestetskii V.B., Lifshitz E.M., Pitaevskii L.P., 1971, *Relativistic quantum theory*, Pergamon press.
Bogovalov S.V., Kotov Yu.D., 1992, *MNRAS*, 257, 537
Bogovalov S.V., 1997, *A&A*, 327, 662
Bogovalov S.V., 1999, *A&A*, 349, 1017
Cheung W.M., Cheng K.S., 1994, *ApJ.(Supplement)* 90, 827
Coroniti F.V. 1990, *ApJ.*, 349, 538
Daugherty J.K, Lerche I., 1975, *Astrophys. and Sp. Sci.*, 38, 437
Daugherty J.K., Harding A.K., 1982, *ApJ*, 252, 337
de Jager O.C., Harding A.K., 1992, *ApJ*, 396, 161
Dermer D., Schlikeiser R., 1991, *A&A*, 252, 414
Goldreich P., Julian W.H., 1969, *ApJ*, 157, 869
Gurevich A.V., Istomin Ia.N., 1985, *ZhETF*, 89, 3
Hester J.J., Scowen P.A., Sankrit R. et al., 1995, *ApJ*, 448, 240
Hillas A.M. et al., 1998, *ApJ*, 503, 744
Kennel C.F., Coroniti F.V., 1984, *ApJ*, 283, 694
Kirk J.G., Ball L., Skjæraasen O., 1999, *Astroparticle Physics*, 10, 31
Kirk J.G., Ball L., 1999, *Astroparticle Physics*, submitted
Knight F.K., 1984, In the Crab Nebula and Related Supernova Remnants, Cambridge university press (Eds. Kafatos M. and Henry R.B.C.), p.27
Lyubarskii Yu.E., 1992, *Sov. Astron. Letters*, 18, 356
Lyubarskii Yu.E., 1996, *A&A*, 311, 172
Mastichiadis A., 1991, *MNRAS*, 253, 235
Middleditch J., Pennypacker C., Burns M.S., 1983, *ApJ*, 273, 261
Nasuti K.P., Mignami R., Caraveo P.A., Bignami G.F., 1996, *A&A*, 314, 849
Nolan P.L., et al., 1993, *ApJ.*, 409, 710
Oke J.B., 1969, *ApJ (letters)*, 156, L49
Percival J.W. et al., 1993, *ApJ*, 407, 276
Rees M.J., Gunn F.E., 1974, *MNRAS*, 167, 1
Romani R.W., Yadigaroglu I.-A., 1995, *ApJ*, 438, 314
Ruderman M., Sutherland P.C., 1975, *ApJ*, 196, 51
Shklovsky I.S. 1968, *Supernovae*, New. York, Wiley,
Stepanian A.A., 1995, *Nucl.Phys. B.*, 39A, 207
Weekes T.C., Aharonian F.A., Fegan D.J., Kifune T., 1997, in Proc. “Fourth Compton Symposium”, Eds. Dermer C.D. et al., AIP Conf. Proc. 410, v. 1, p. 361
Weekes T.C. et al., 1998, in Proc. “Neutron Stars and Pulsars”, Eds. N.Shibazaki, N. Kawai, S. Shibata, T. Kifune, Universal Academy Press, Tokyo, p. 465

APPENDIX A: OPACITY OF THE MAGNETIC FIELD OF THE WIND FOR THE TEV PHOTONS.

In the paper of (Cheung & Cheng 1994) it was argued that TeV photons produced near the light cylinder of the Crab pulsar will be absorbed, because of conversion of these photons in e^\pm pairs in nonuniform magnetic field. We show here that accurate estimate of the rate of the conversion of photons in pairs taking into account electric field existing in the wind give negligible absorption of TeV gamma-rays produced via IC scattering.

The motion of the wind occurs under frozen in condition. Particles move not only along field lines, but there is

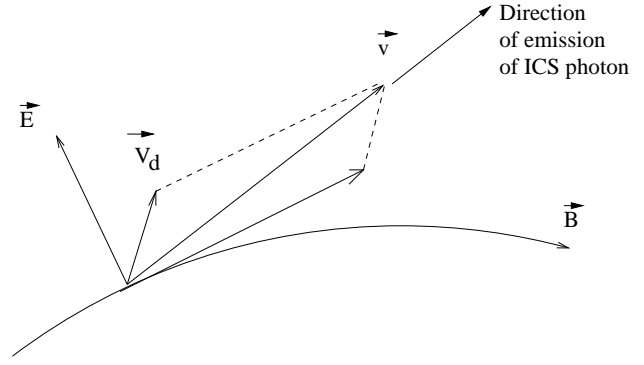


Figure A1. The geometry of the MHD plasma flow.

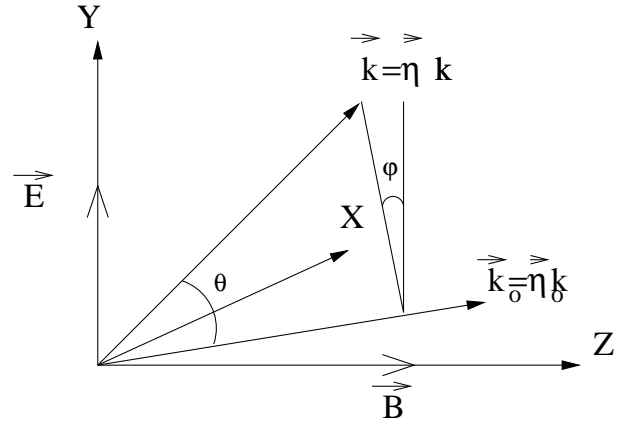


Figure A2. The geometry used in equation (A2).

component of the velocity \mathbf{V}_d directed perpendicular to the magnetic field line. This is so called drift velocity defined by the expression

$$\mathbf{V}_d = \frac{\mathbf{E} \times \mathbf{B}}{B^2} \quad (\text{A1})$$

V_d is comparable with c beyond the light cylinder, where the electric and magnetic fields are of the same order. The schematic relationship between the magnetic and electric fields and the velocity of plasma is shown in Fig. A1. In this situation an energetic photon is emitted along the velocity vector of the particle at large angle to the magnetic field. However, this happens in the region of crossed electric and magnetic fields, where the coefficient of absorption of the photon is modified by the electric field. The probability of conversion of the photon on unit length, taking into account the electric field, was defined by Daugherty & Lerche: (1975)

$$\xi = 0.23\alpha \frac{mc}{\hbar} \frac{B\chi}{B_{cr}} \frac{(1 - E^2/B^2)}{(1 - E\eta_x/B)} \exp\left(-\frac{8}{3} \frac{B_{cr}}{E_\gamma \chi B}\right), \quad (\text{A2})$$

where

$$\chi = \sqrt{(\eta_x - \frac{E}{B})^2 + \eta_y^2(1 - \frac{E^2}{B^2})}, \quad (\text{A3})$$

and $\alpha = 1/137$. η_x and η_y are the components of the unit vector directed along the velocity of the photon as it is shown in Fig. A2 and E_γ is the energy of photon expressed in units of mc^2 .

The components of the velocity of the particle in the

system of coordinates presented in Fig. A2 are as follows $v_x = \frac{cE}{B}$, $v_y = 0$, $v_z = c\sqrt{1 - \frac{E^2}{B^2}}$. The corresponding components of the unit vector η of the photon at the place of the emission will be $\eta_x = \frac{v_x}{v} = \frac{E}{vB}$, $\eta_y = 0$, $\eta_z = \sqrt{1 - \eta_x^2}$. Substitution of these components in equation (A3) gives us

$$\chi = \frac{E}{B} \frac{c}{\gamma^2(1 + v/c)v} \quad (\text{A4})$$

This factor is extremely small, $\chi \sim 10^{-14}$, for the expected parameters of the wind.

Photons propagate along straight lines. Charged particles move in electromagnetic fields and their trajectories diverge from straight lines. If photon would moved along the trajectory of the charged particles, they would never convert in pairs. Therefore it is clear that the probability of conversion of a photon into a pair basically depends on the radius of curvature R_c of the trajectory of the charged particles, but not the magnetic field.

The angle ϑ between the direction of propagation of the photon and direction of propagation of the emitting electron depends on the path length of the photon l ;

$$\vartheta = \frac{l}{R_c}. \quad (\text{A5})$$

The dependence of components of the vector η on θ is as follows

$$\eta_x = \eta_{x0} \cos \vartheta + \eta_{z0} \sin \vartheta \sin \varphi \quad (\text{A6})$$

$$\eta_y = \sin \vartheta \cos \varphi \quad (\text{A7})$$

Neglecting by terms of the order $1/\gamma^2$ and $\sin^n \vartheta$ in powers higher than 2, we obtain the following estimate for χ at small θ

$$\chi \sim \frac{l}{R_c} \sqrt{1 - \left(\frac{E}{B}\right)^2}. \quad (\text{A8})$$

As we are interested in the maximal values of χ , we can neglect the term $\sqrt{1 - \left(\frac{E}{B}\right)^2}$ in this expression. Assuming that after the light cylinder the total magnetic field decreases as $1/r$, we obtain for the function $q = \frac{8B_{cr}}{3E_\gamma B_\gamma \chi}$ the following estimate of the upper limit

$$q = \frac{8B_{cr}R_c}{3E_\gamma B_{lc}r_L}, \quad (\text{A9})$$

and for the probability of conversion of the photon into a pair we obtain finally the estimate

$$\xi \leq 0.23\alpha \frac{mc}{\hbar} \frac{B_{lc}r_L}{B_{cr}R_c} \exp\left(-\frac{8B_{cr}R_c}{3E_\gamma B_{lc}r_L}\right) \quad (\text{A10})$$

where B_{lc} is the magnetic field on the light cylinder and R_c is also taken on the light cylinder.

The solution of the problem of the relativistic wind flows in the model of an axisymmetrically rotating star allows us to estimate the radius of curvature R_c of the trajectories of the particles in the wind (Bogovalov 1997) as

$$\frac{1}{R_c} = \frac{\sigma_w}{\gamma^2 r}. \quad (\text{A11})$$

This estimate shows that the radius of curvature of the trajectories of particles is much more than the curvature radius of the magnetic field line, which is of the order r . Such a large curvature radius gives $q \gg 1$ for almost any parameters of the wind. This is why the IC photons produced in

the wind are not converted into pairs even at energies ~ 100 TeV and $\sigma_w \sim 1$.